ACS APPLIED MATERIALS & INTERFACES

www.acsami.org

Research Article

Insights into Excitonic Dynamics of Terpolymer-Based High-Efficiency Nonfullerene Polymer Solar Cells: Enhancing the Yield of Charge Separation States

Jianfeng Li,*# Zezhou Liang,# Xiaoming Li, Hongdong Li, Yufei Wang, Jicheng Qin, Junfeng Tong, Lihe Yan,* Xichang Bao,* and Yangjun Xia

Cite This: *ACS Appl. Mater. Interfaces* 2020, 12, 8475−8484

Read Online

ACCESS | Metrics & More | Article Recommendations | Supporting Information

ABSTRACT: Ternary copolymerization strategy is considered an effective method to achieve high-performance photovoltaic conjugated polymers. Herein, a donor−acceptor1−donor−acceptor2-type random copolymer, named PBDTNS-TZ-BDD (T1), containing one electron-rich unit alkylthionaphthyl-flanked benzo[1,2-*b*/4,5-*b*′] di-thiophene (BDTNS) as D and two electron-deficient moieties benzo[1,2-*c*/4,5-*c*′]dithiophene-4,8-dione (BDD) and fluorinated benzotriazole as A, was synthesized to investigate the excitonic dynamic effect. Also, the D−A-type alternating copolymer PBDTNS-BDD (P1) was also prepared for a clear comparison. Although the UV−Vis spectra and energy levels of P1 and T1 are similar, the power conversion efficiencies (PCEs) of the related devices are 11.50% (T1/ITIC) and 8.89% (P1/ITIC), respectively. The reason for this is systematically investigated and analyzed by theoretical calculation, photoluminescence, and pump-probe transient absorption spectroscopy. The density functional theory (DFT) and time-dependent density functional theory (TD-DFT) calculation results show that the terpolymer T1 with a lower exciton binding energy and a longer lifetime of spontaneous luminescence can synergistically increase the number of excitons reaching the donor/acceptor interface. The results of the pump-probe transient absorption spectroscopy show that the yield of charge separation of T1/ITIC is higher than that of the P1/ITIC blend film, and improved PCE could be achieved via copolymerization strategies. Moreover, the fabrication of the T1-based device is also simple without any additive or postprocessing. Therefore, it provides a promising and innovative method to design high-performance terpolymer materials.

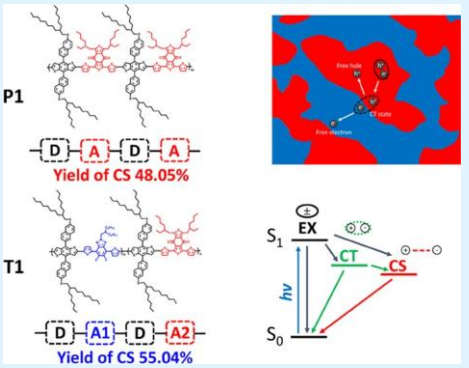

KEYWORDS: *copolymerization strategy, DFT and TD-DFT, photophysics, pump-probe transient absorption spectroscopy, polymer solar cells*

1. INTRODUCTION

The power conversion efficiency (PCE) of the polymer solar cells (PSCs) has increased from less than 1% to more than 16% in recent decades.[1−14] Over the years, alternating donor−acceptor polymers have been primarily developed to expand the absorption and harvest more solar energy.[15−22] A lot of effort has been devoted to optimize the energy levels, absorbance, molecular stacking, adjusting solubility, and designing new donor (D) or acceptor (A) units.[23,24] Recently, random terpolymer strategy has been considered to be an effective method without a complicated design to regulate spectral absorption, energy level, and nanostructure and achieve the morphological control of the active layer.[25−27] For example, triblock copolymers are formed by inserting a D unit or an A unit, which integrates the advantage of each unit.[28−30]

Recently, the binary PSCs based on terpolymer with PCE of more than 15% were obtained by introducing an ester-substituted thiophene unit into benzo[1,2-*b*/4,5-*b*′]dithiophene BDT-benzo[1,2-*c*/4,5-*c*′]dithiophene-4,8-dione (BDD) alternating polymer PBDB-TF to improve the electron-withdrawing performance of host blocks, showing its great potential for development. The D−A1−D−A2 terpolymer was synthesized using BDT as the D unit and benzothiadiazole (BT) and diketopyrrolopyrrole (DPP) as the A unit, and a stable large-area PSC with PCE of over 13% was realized.[31] This strategy can easily adjust the energy level and absorption spectrum of terpolymer by controlling the D/A unit ratio in the polymer backbone.[32] Also, the crystallization and microphase separation of the copolymer could be modulated by random copolymer methods.[33] Furthermore, the fine-tuning solid-state packing of the photoactive layer could remarkably improve the photovoltaic characteristics through side-chain engineering using

Received: November 9, 2019
Accepted: January 22, 2020
Published: January 22, 2020

random polymerization.[34] The copolymerization strategy shows great potential to improve the photovoltaic performance and practical application, so it is necessary to investigate it more deeply.

Herein, a terpolymer named PBDTNS-TZ-BDD (hereinafter referred to as T1) was synthesized by introducing the fluorinated-benzotriazole (FBTA) acceptor building block unit into the alternating polymer PBDTNS-BDD (hereinafter referred to as P1) (Figure 1a).[35] The PCE of PSC-based

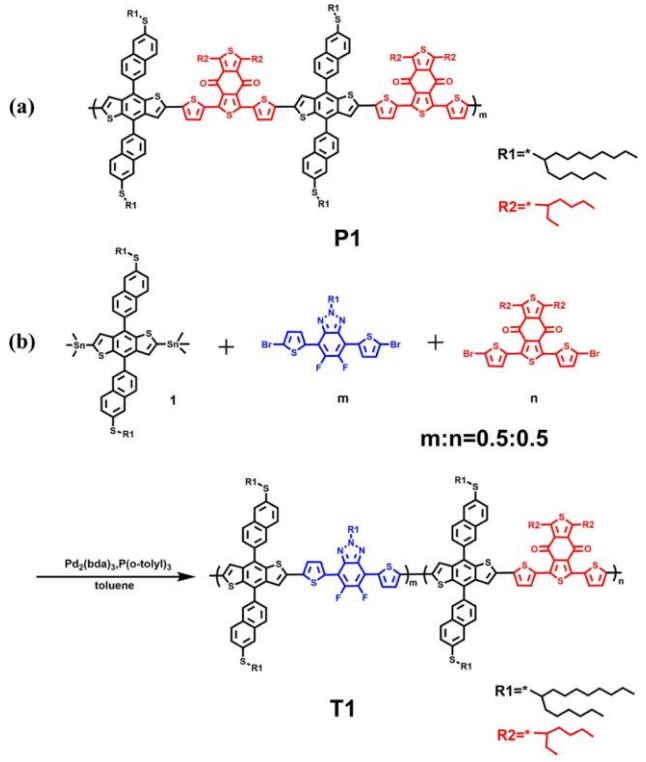

Figure 1. (a) Chemical structure for P1. (b) Synthetic routes of the random copolymer T1.

PBDTNS-BDD/ITIC is 8.89%. Surprisingly, the terpolymer T1 is very easy to dissolve in most common solvents, and the PCE of the PSCs based on T1/ITIC exceeds 11% without any post-treatments (additives or thermal annealing). The reason is systematically investigated and analyzed by theoretical calculation, photoluminescence (PL), and pump-probe transient absorption spectroscopy (TAs). The calculated reforsults of density functional theory (DFT) and time-dependent density functional theory (TD-DFT) suggest that T1 with a smaller exciton binding energy (E_b) is favorable to exciton split and a longer lifetime of spontaneous luminescence that could synergistically increase the number of excitons reaching the donor/acceptor interface. The measurements of TAs show that the yields of charge separation (CS) are higher in T1/ITIC than that in the P1/ITIC blend film. The introduction of FBTA could break the periodic ordering of the main chain of polymers to optimize the solubility and miscibility with ITIC and obtain a better morphology.

2. RESULTS AND DISCUSSION

2.1. Synthesis and Characterization. P1 was synthesized according to previous work,[32] and the synthetic route of terpolymer T1 is shown in Figure 1b. The detailed synthesis process and characterization are exhibited in the Supporting Information. The number-average molecular weights (M_{ns}) and polydispersity indexes (PDIs) of P1 and T1 are 27 and 25 kDa and 1.90 and 2.10, respectively (Table 1). T1 shows good

Table 1. Molecular Weights and Optical and Electrical Characteristic

polymers	M_{ns} (kDa)	PDI	λ_{max} (nm)	E_g^{opt} [eV]	HOMO (eV)	LUMO (eV)
P1	27	1.90	624	1.84	−5.32	−3.48
T1	25	2.10	596	1.86	−5.40	−3.54

[a] $E_g^{opt} = 1240/\lambda_{onset}$.

thermal stability and a decomposition temperature (T_d) higher than 360 °C (Figure S1). The absorption spectra of the pure polymers and D/A blend films were recorded (Figures 2a and S2). The maximum absorption peaks for P1 and T1 are 624 and 596 nm, respectively. Also, the two polymers have the same E_g^{opt} (~1.85 eV). The E_{HOMO} (energy level of the highest occupied molecular orbital) and E_{LUMO} (energy level of the lowest unoccupied molecular orbital) levels of P1 and T1 have been studied by cyclic voltammetry method. After incorporating FBTA into the polymer backbone, the E_{HOMO} and E_{LUMO} were pulled down as a whole. Also, the deeper HOMO of the random copolymer T1 would be beneficial to achieving a higher open-circuit voltage (V_{OC}).

2.2. Photovoltaic Characteristics. For a more in-depth study of the performance of random polymers, the PSCs based on P1 and T1 were fabricated without any additive or postprocessing. Their current density−voltage ($J-V$) curves and the photovoltaic characteristic parameters are given in Figure 2c and Table 2. The V_{OC}, J_{SC}, fill factor (FF), and PCE for the PSC (P1/ITIC) are 0.940 V, 14.99 mA cm^{-2}, 63.12%, and 8.89%, respectively, which are close to the values reported in the literature.[24] The PSC based on T1/ITIC shows better performance (V_{OC} = 0.952 V, J_{SC} = 16.80 mA cm^{-2}, FF = 71.91%, and PCE = 11.50%) than that based on P×The J_{sat} of1/ITIC. In the wavelength range of 500−700 nm (Figure 2b), the external quantum efficiency (EQE) of PSCs (T1/ITIC) is higher than that of PSCs (P1/ITIC), which is consistent with the higher J_{SC} of PSCs (T1/ITIC).

To further understand the photocurrent behavior, the relationship between effective voltage (V_{eff}) and photocurrent (J_{ph}) was also investigated (Figure 2d).[36−38] J_{sat} of PSCs (T1/ITIC) is larger than that of PSCs (P1/ITIC). The charge dissociation probability (P(E,T)) can be obtained by P(E,T) = J_{ph}/J_{sat}.[39] The P(E,T) of the T1-based device is more than 98% under the short-circuit condition, indicating that it has excellent charge dissociation probability. To understand charge transport properties, the hole (μ_h) and electron (μ_e) mobilities were calculated by the space-charge-limited (SCLC) method (as shown in Figure S5).[40−43] The values of μ_h and μ_e of T1-based devices are 2.03 × 10^{-4} and 1.94 × 10^{-4} cm^2 V^{-1} s^{-1}, respectively. However, the values of μ_h and μ_e of P1-based devices are 3.51 × 10^{-4} and μ_e = 1.73 × 10^{-4} cm^2 V^{-1} s^{-1}, respectively, with the former having higher mobility than the latter. In addition, T1-based devices have a more balanced μ_h/μ_e, which is beneficial to carrier transport.[44,45] The recombination properties of electrons and holes with one another in their mutual Coulombic field are critical for the carrier losses and eventual photocurrent.[46,47] Generally, the actual recombination

https://dx.doi.org/10.1021/acsami.9b20364
ACS Appl. Mater. Interfaces 2020, 12, 8475−8484

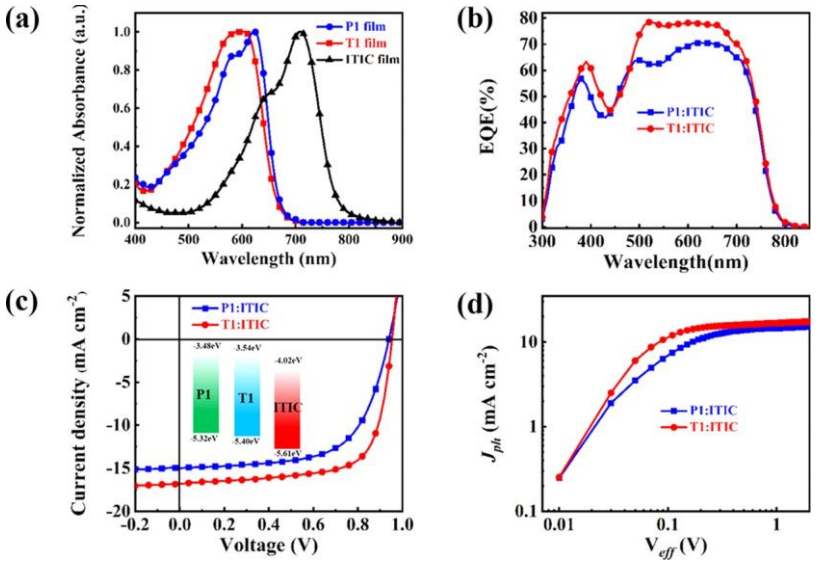

Figure 2. (a) Absorbance of the pure P1 and T1 films. (b) EQE and (c) $J-V$ curves. Inset is the energy level diagram (eV) of P1, T1, and ITIC. (d) $J_{ph}-V_{eff}$ curves of the P1/ITIC (1:1)- and T1/ITIC (1:1)-based PSCs.

Table 2. Photovoltaic Characteristic of PSCs

devices	V_{OC} [V]	J_{SC} [mA cm^{-2}]	FF [%]	PCE[a] [%]	R_S (Ω cm^2)	R_{SH} (Ω cm^2)
P1/ITIC	0.940 (±0.01)	14.99 (±0.35)	63.12 (±0.47)	8.89 (±0.25)	8.53	1484.78
T1/ITIC	0.952 (±0.01)	16.80 (±0.28)	71.91 (±0.31)	11.50 (±0.33)	4.92	1760.03

[a]Average values from 15 devices.

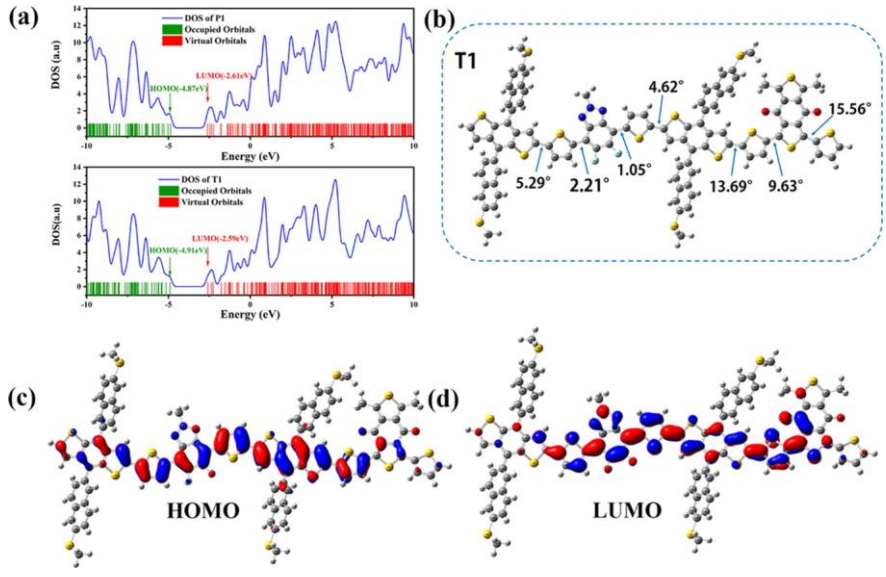

Figure 3. (a) DOS of copolymers P1 and T1. (b) Optimized structure of the molecular simplified model of copolymer T1. (c, d) Molecular wave function distributions of the frontier orbits of T1.

coefficient (β) in bulk heterojunction PSCs could be ascribed as eq 1[46,48]

$$\gamma = \beta/K_L \quad (1)$$

where K_L is the Langevin rate constant and γ is a dimensionless parameter.[30] γ can be obtained by eq 2

$$\gamma = \frac{16\pi}{9} \times \frac{\mu_e\mu_h}{\mu_{double}^2 - (\mu_e + \mu_h)^2} \quad (2)$$

$$K_L = \frac{q}{\varepsilon_0\varepsilon_r}(\mu_e + \mu_h) \quad (3)$$

where μ_{double}, μ_e, and μ_h are the effective, electron, and hole mobilities of the double-carrier device;[47,49] q is the basic charge; and $\varepsilon_0\varepsilon_r$ is the dielectric constant of the blend films. The K_L for T1- and P1-based devices could be calculated as 3.16×10^{-10} and 2.39×10^{-10} cm^{-3} s^{-1}, respectively, under eq 3. According to the μ of single- and double-carrier devices (Figure S6), the γ values were extracted to be 3.57×10^{-1} and 1.07×10^{-1} for the P1- and T1-based PSCs, respectively. The β of T1-based devices

https://dx.doi.org/10.1021/acsami.9b20364
ACS Appl. Mater. Interfaces 2020, 12, 8475−8484

Table 3. Calculated ΔE_{H-L}, First Singlet Excitation Energy (E_{S1}), Binding Energy (E_b), Composition, Main Transition Contribution (%), Absorption Wavelength (λ), and Oscillator Strength (f) of the Molecules for P1 and T1

molecule	ΔE_{H-L} (eV)	E_{s1} (eV)	E_b (eV)	E_{if} (cm^{-1})	state	composition[a]	λ_{max} (nm)	f
P1	2.270	1.997	0.491	16 112.538	$S_0 \rightarrow S_1$	H to L (84.33%)	620.36	3.755
					$S_0 \rightarrow S_3$	H to L + 2 (67.99%)		0.362
T1	2.330	2.072	0.244	16 708.582	$S_0 \rightarrow S_1$	H to L (91.42%)	598.50	3.189
					$S_0 \rightarrow S_3$	H to L + 2 (79.77%)		0.091

[a]H represents HOMO, L represents LUMO.

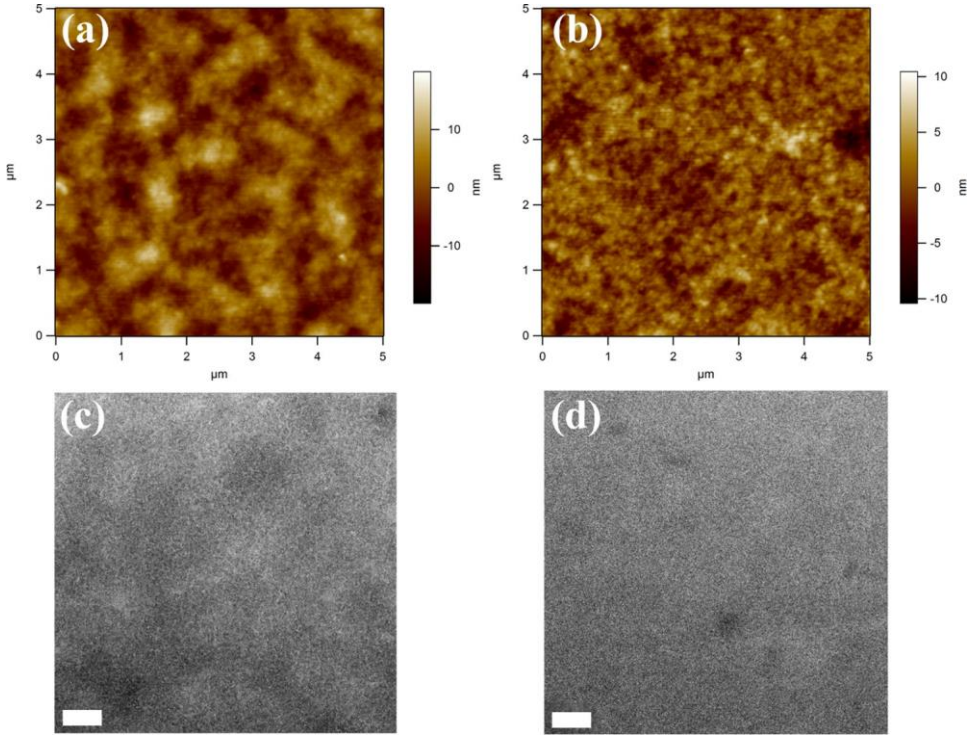

Figure 4. AFM height images of (a) P1/ITIC and (b) T1/ITIC blend films. Corresponding TEM images of (c) P1/ITIC and (d) T1/ITIC blend films (the scale bar represents 200 nm).

(1.29×10^{-10} cm^{-3} s^{-1}) is lower than that of P1-based devices (2.57×10^{-11} cm^{-3} s^{-1}), which indicates that the recombination degree and carrier loss are less in T1-based solar cells.

2.3. DFT Calculations. For a more in-depth understanding of P1 and terpolymers T1, DFT calculations were employed to optimize structures, simulate the electron spectrum, and calculate exciting energies and oscillator strengths of the two molecules, as displayed in Figures 3 and S4. To better simulate the physical and chemical properties of the terpolymers T1, a D−A1−D−A2 simplified model was chosen. Furthermore, a D−A−D−A simplified model for P1 is also evaluated. Also, the solvent effect (chlorobenzene, the solvent used in the experiment) was described with a nonequilibrium implementation of the conductor-like polarizable continuum model (C-PCM) to simulate the actual environment of the molecule.[50] The geometries of P1 and T1 were optimized at the B3LYP-D3(BJ)/6-31G(d) level.[51,52] The optimization geometry and the density of states (DOS) curve can help us better understand the electronic properties of two polymers, as shown in Figure 3a. The energy gap values are 2.26 eV (P1) and 2.32 eV (T1), respectively, and the increasing trend from P1 to T1 is highly consistent with the experimental data. The calculated maximum absorption peaks of P1 and T1 are 620.36 and 598.50 nm, respectively, which agree well with the experimental data (Figure 2a); this is consistent with the $S_0 \rightarrow S_1$ transition that mainly comes from a single one-electron excitation from HOMO(H) → LUMO(L). In the two molecules, the relative lower-energy absorption band and the wave function distributions of the frontier orbits are π−π* type (Figure 3c,d), indicating there exists an obvious intramolecular charge transfer (ICT) effect.

According to the basic physical mechanism of photovoltaic devices, excitons are generated in the blend film by absorbance of light by donor or acceptor materials (here we focus more on donor materials), diffusion, and dissociation at the donor/acceptor interface. The exciton binding energy (E_b) is an important basic parameter determining the photoelectric properties of photovoltaic materials and devices.[53,54] Also, the hole−electron pairs do not directly split into free charge carriers, as they are bound by Coulombic attraction, which results in a large exciton binding energy (E_b).

E_b is the energy barrier that charges have to overcome to escape from the D/A interface and migrate toward the electrode and is directly related to the charge separation in PSCs. In general, E_b can be expressed as[4,55]

$$E_b = \Delta E_{H-L} - E_{S1} \quad (4)$$

where ΔE_{H-L} is the offset between HOMO and LUMO energy levels at the S_0 state and E_{S1} is the energy of the first singlet

https://dx.doi.org/10.1021/acsami.9b20364
ACS Appl. Mater. Interfaces 2020, 12, 8475−8484

excitation for the molecules; these can be obtained by the B3LYP/6-31G(d) and TD-PBE0/6-31G(d) levels, respectively. The results of DFT calculation are summarized in Table 3. T1 with a smaller E_b is more likely to split exciton than P1, increasing the possibility of free carriers. In addition, the exciton diffusion ability is related to its diffusion length (L_D).[56] A longer L_D will be beneficial to the higher exciton diffusion efficiency, which requires a longer exciton lifetime τ (ns).[57] Here, τ value is close to the lifetime of spontaneous radiation, which can be assessed by the Einstein spontaneous emission relationship5[57,58]

$$\tau = 1.499\frac{1}{f \times E_{ff}^2} \quad (5)$$

where f is the oscillator strength and E_{if} is the excitation energy in cm^{-1}. The τ of T1 (1.68 ns) is longer than P1 (1.53 ns), so the longer lifetime of spontaneous emission will increase the L_D and then increase the number of excitons reaching the D/A interface.

2.4. Morphological Analysis. The fine morphology of the film is a critical condition to achieve high-performance PSCs. Atomic force microscopy (AFM) with the tapping mode and transmission electron microscopy (TEM) were employed to investigate the surficial and internal morphologies of P1- and T1-based blend films. As shown in Figure 4, although the surfaces of the two polymer blend films are quite uniform, the root-mean-square roughness (RMS) of the P1/ITIC blend film (4.026 nm) is higher than that of the T1/ITIC blend film (2.024 nm), which might be due to the high crystallization tendency of P1. The TEM images maintain a high degree of consistency with the AFM results. The T1/ITIC blend film displays moderate aggregation and desirable morphologies, which can enhance exciton dissociation efficiencies. The blend films were well mixed without any obvious self-aggregation, this good miscibility is favorable for forming appropriate phase separation and thus leads to higher FF.

2.5. Photophysical Property. For a more in-depth understanding of the magnitude of intermixing in polymers/ITIC (D/A = 1:1) blend films, the PL measurements were employed to probe the PL of neat P1 and T1 films and PL quenching (PLQ) in their blend films. PLQ was calculated as6[59]

$$PLQ = 1 - PL_{blend}/PL_{neat} \quad (6)$$

The exciton diffusion distance L can be estimated by the degree of the PLQ in blend films, which can be calculated by eq 7[59,60]

$$L = L_{ex}(1 - PLQ)^{1/2} \quad (7)$$

where L_{ex} is the exciton diffusion length in pure film, and its typical value for neat narrow band gap polymers was usually assumed to be 10 nm.[61] Here, we only give the relative expression of L occurring in the blend films. To analyze the mixed system more closely, the finite size of the exciton was neglected.[60] We also assume efficient quenching when a polymer exciton arrived at ITIC molecules. As shown in Figure 5, the emission of P1 and T1 in polymers/ITIC blends is highly quenched (92.23% for P1 and 98.78% for T1 compared to their respective neat materials). According to eq 7, the exciton diffusion distance L between P1 and T1 in the blend films can be estimated to be 2.78 and 1.10 nm, respectively. Such short diffusion distances indicate a high degree of ITIC mixing in the polymer-rich regions.[60] So, a smaller L of the T1/ITIC blend film may suggest a better mixture, which is also consistent with the results observed in AFM and TEM. The excitons generated by polymer could be more effective and directly adjacent to an

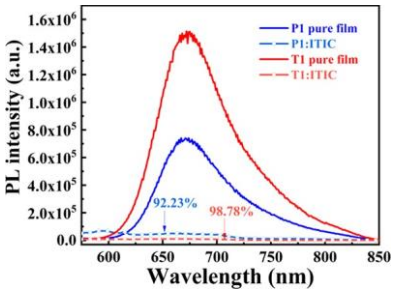

Figure 5. Steady-state PL of pure P1 and pure T1 and their respective blend films (D/A = 1:1) excited under 600 nm.

ITIC molecule in the T1/ITIC blend film. Therefore, the introduction of FBTA unit can break the periodic order of the polymer skeleton, which could be beneficial to optimize the solubility and miscibility with ITIC while maintaining the electrical properties and polymer packing in sold state.[62]

Apart from the above tests, the exciton and polaron kinetics of the ground and excited states of pure and blend films with ITIC were studied using TAs. The TA spectra customarily have two main features: GSB (ground-state bleach) and ESA (excited-state absorption signal) characteristics. First, the pure P1 and T1 films were studied by ultrafast TAs, as shown in Figure 6. The ultrafast TAs of pure polymer films P1 and T1 exhibited negative GSB signals in the range of 500−640 nm, which is consistent with the polymers' static electronic spectra and could be identified as a singlet exciton transition. The ESA bands of P1 and T1 scattered among 640−750 nm with panning polaron absorption (PA) range of 850−1000 nm were singlet exciton induced. Under the circumstance of neat film P1 at ∼0.1 ps, the GSB intensity is nearly 17 mOD and the homologous ESA and PA are ∼5 mOD and ∼3 mOD. Meanwhile, the pure T1 film exhibited the GSB signal with ∼36 mOD, where the equivalents ESA and PA characteristics are ∼28 mOD and ∼17 mOD. The corresponding characteristic peak intensity of T1 is higher than that of the counterpart (neat P1 and T1 films were measured with a uniform thickness). Based on the above discussion, it can be inferred that the exciton yield of primary TA signals was higher in T1, which corresponds well with that of PL signals in pure polymers (as shown in Figure 5).

We further used TA measurements to investigate the electron transfer (ET) process in P1/ITIC and T1/ITIC blend films.[45] The GSB signals of two films covered a range of 500−740 nm, and the $\Delta A/A$ spectra exhibit the characteristics of neat P1 and T1 films pumped at 400 nm, for $\Delta t > 1$ ps (as displayed in the Supporting Information, Figure S7). The measured TA spectra are shown in Figure S8, and the GSB peak is 710 nm. The new features are attributed to the GSB of ITIC, suggesting that both blends have efficient ET processing.[63] Also, for the near-infrared region with ESA signature, which could be attributed to the charge-transfer (CT) state and charge-separated (CS) state.[64] The underlying exciton decay dynamics of the binary system could be studied with singular value decomposition (SVD) fitting method from the overlapped TA spectra. The SVD-fitted TA spectra of binary blends are shown in Figure 7c,d. Figure 7d shows species-associated difference spectra of T1, and the SVD fitting results extracted three components with a lifetime of 1.55 ps (black), 23.30 ps (red), and 677 ps (blue), respectively. We noted that in this 23.30 ps component, the spectral characteristics of a negative bleach at ∼600 nm are different from those in the pure P1 film (as shown in Figure 6), which is a signature

https://dx.doi.org/10.1021/acsami.9b20364
ACS Appl. Mater. Interfaces 2020, 12, 8475−8484

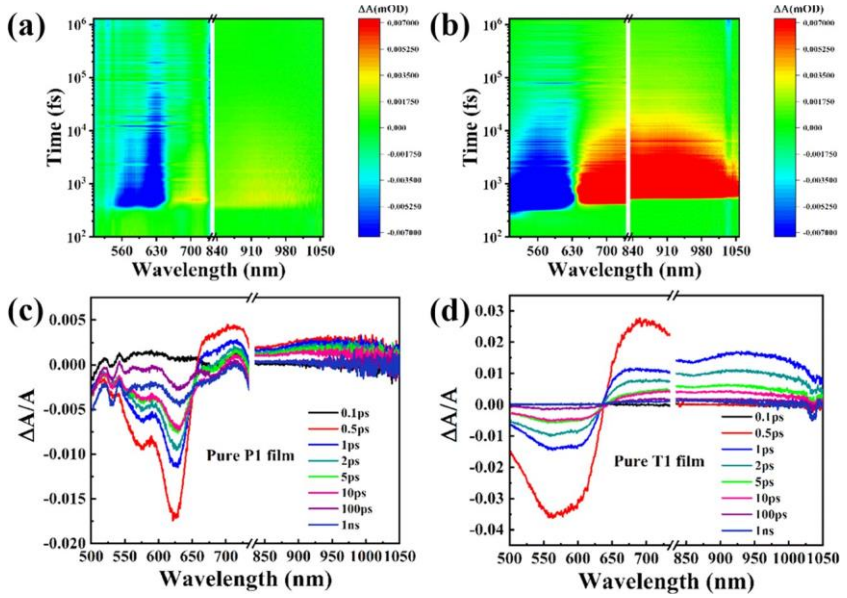

Figure 6. (a, c) TA spectra of neat P1 films. (b, d) TA spectra of neat T1 films. All the films are pumped at 400 nm.

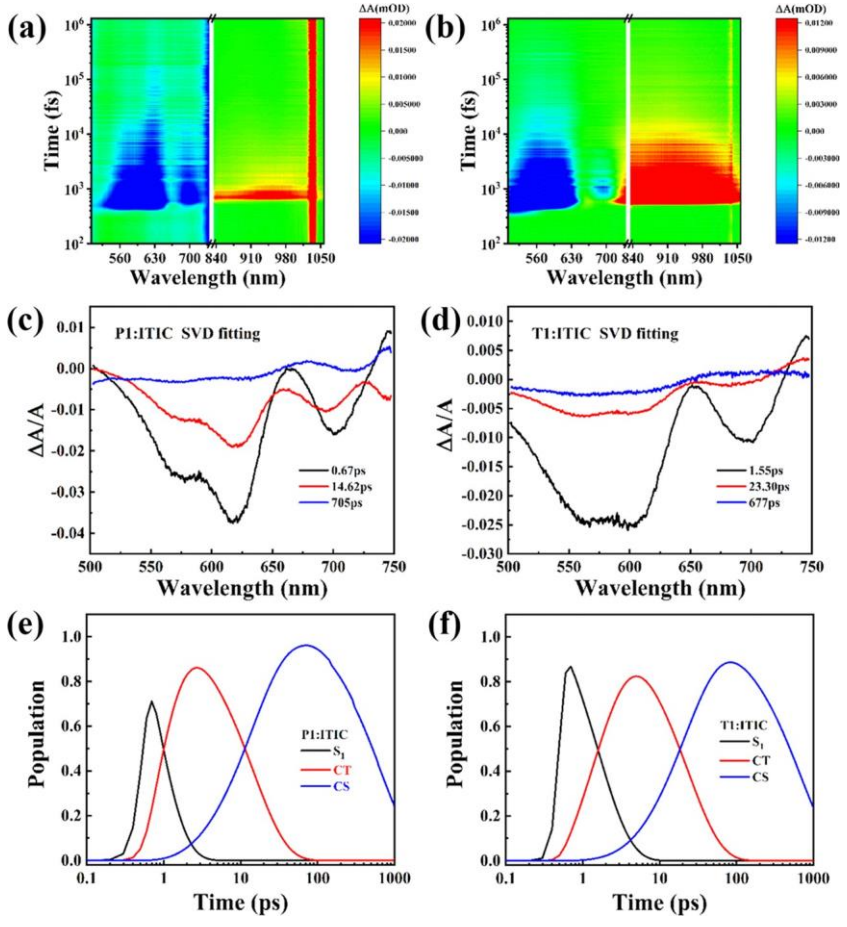

Figure 7. (a, b) TA spectra recorded from the P1/ITIC and T1/ITIC films. (c, d) Species-associated difference spectra of the TA spectra by SVD fitting recorded profile from the P1/ITIC and T1/ITIC films, all the films are pumped at 400 nm. (e, f) Population−time curve.

feature of the intermediate CT state where the holes are not directly injected into the HOMO energy level of P1.[64,65] The 1.55 ps component was denoted for hole transfer to T1 directly from the photoexcitation in ITIC leads to the formation of the interfacial CT state. The CS state produced by intermolecular exciton splitting (or charge transfer) was probed in the T1/ITIC blend film with a weak Coulombic binding force at the D/A interface, as shown in Figure 8a,b. A new feature of the bleach character appeared at 560 nm in the spectrum signal of the CS state corresponding with CT/photoinduced exciton (EX)

https://dx.doi.org/10.1021/acsami.9b20364
ACS Appl. Mater. Interfaces 2020, 12, 8475−8484

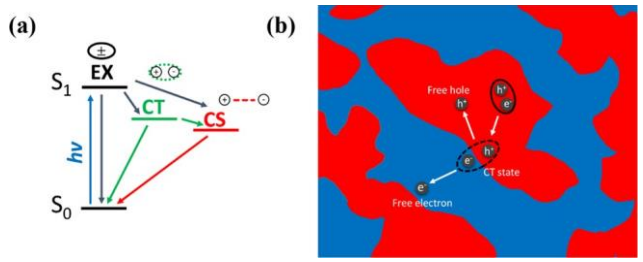

Figure 8. (a) Analyzed target model of charge generated. (b) Schematics of charge transportation pathways in binary blend film.

occurs, that paired well with the GSB character of the pure T1, indicating an efficient splitting of h−e pairs. Also, similar processes have been probed in the P1/ITIC blend film, and the lifetimes of the three components were extracted as 0.67 ps (black), 14.62 ps (red), and 705 ps (blue), respectively. The target analysis model and exciton dissociation model in the polymer/ITIC blend are shown in Figure 8a,b. As shown in Table S1, the evolution of the corresponding amplitude for each component was summarized, and the yields of CS states could be easily calculated by8[57]

$$\Phi_{CS} = A_{EX\rightarrow CT} \times A_{CT\rightarrow CS} + A_{EX\rightarrow CS} \quad (8)$$

The yield of CS (electron) in the T1/ITIC blend film is 55.04%, which is much higher than that of P1/ITIC (48.05%), confirming the fact that a better PCE was achieved in T1/ITIC-based devices. These dynamic studies strongly support the fact that ternary copolymerization strategies could enhance the CS yields and then produce a better FF and a higher J_{SC} global performance of the devices under the same situation.

3. CONCLUSIONS

A random terpolymer T1 was synthesized using ternary copolymerization strategies by introducing FBTA into the PBDTNS polymer, and J_{SC} and V_{OC} of PSCs were improved synchronously and 11.50% PCE was obtained. The calculated results of DFT and TD-DFT show the terpolymer T1 with a lower exciton binding energy and a longer lifetime of spontaneous luminescence, which could synergistically increase the number of excitons reaching the donor/acceptor interface. Pump-probe technology was employed to unveil the excitonic dynamics of the two polymers. The exciton concentration of the initial transient signal was higher in neat T1 film, and the production of a charge-separated (CS) in the T1/ITIC blend film was higher than that in the P1/ITIC film, which could produce more charges. Moreover, the fabrication of the T1-based device is also simple without any additive or postprocessing. The fine morphology of blend film could be beneficial for a higher PCE. Therefore, it provides a promising and innovative strategy to design high-performance terpolymer.

4. EXPERIMENTAL SECTION

Experiment material, synthesis, fabrications of device, and measurements are provided in the Supporting Information.

ASSOCIATED CONTENT

Supporting Information

The Supporting Information is available free of charge at https://pubs.acs.org/doi/10.1021/acsami.9b20364.

Materials; synthesis of polymers; instruments and measurements; device fabrication and characterization; TGA plots of T1; normalized absorption spectra; cyclic voltammetry (CV); optimized structure of the molecular; hole and electron mobility measurement; transient absorption and pump-probe measurements and TA spectra; and global fitting parameters (Figures S1−S7 and Table S1) (PDF)

AUTHOR INFORMATION

Corresponding Authors

Jianfeng Li − *School of Materials Science and Engineering, Lanzhou Jiaotong University, Lanzhou 730070, P. R. China;* orcid.org/0000-0002-1361-4381; Email: ljfpyc@163.com

Lihe Yan − *Key Laboratory for Physical Electronics and Devices of the Ministry of Education & Shaanxi Key Lab of Information Photonic Technique, School of Electronics and Information Engineering, Xi'an Jiaotong University, Xi'an 710049, P. R. China;* orcid.org/0000-0001-9860-597X; Email: liheyan@mail.xjtu.edu.cn

Xichang Bao − *Qingdao Institute of Bioenergy and Bioprocess Technology, Chinese Academy of Sciences, Qingdao 266101, P. R. China;* orcid.org/0000-0001-7325-7550; Email: baoxc@qibebt.ac.cn

Authors

Zezhou Liang − *School of Materials Science and Engineering, Lanzhou Jiaotong University, Lanzhou 730070, P. R. China; Key Laboratory for Physical Electronics and Devices of the Ministry of Education & Shaanxi Key Lab of Information Photonic Technique, School of Electronics and Information Engineering, Xi'an Jiaotong University, Xi'an 710049, P. R. China*

Xiaoming Li − *Qingdao Institute of Bioenergy and Bioprocess Technology, Chinese Academy of Sciences, Qingdao 266101, P. R. China; College of Chemistry and Pharmaceutical Engineering, Hebei University of Science and Technology, Shijiazhuang 050018, P. R. China*

Hongdong Li − *Key Laboratory of Eco-chemical Engineering, College of Chemistry and Molecular Engineering, Qingdao University of Science and Technology, Qingdao 266042, P. R. China*

Yufei Wang − *School of Materials Science and Engineering, Lanzhou Jiaotong University, Lanzhou 730070, P. R. China*

Jicheng Qin − *School of Materials Science and Engineering, Lanzhou Jiaotong University, Lanzhou 730070, P. R. China*

Junfeng Tong − *School of Materials Science and Engineering, Lanzhou Jiaotong University, Lanzhou 730070, P. R. China*

Yangjun Xia − *School of Materials Science and Engineering, Lanzhou Jiaotong University, Lanzhou 730070, P. R. China*

Complete contact information is available at: https://pubs.acs.org/10.1021/acsami.9b20364

Author Contributions

#J.L. and Z.L. contributed equally to this work.

Notes

The authors declare no competing financial interest.

ACKNOWLEDGMENTS

The authors thank the National Natural Science Foundation of China (No. 61964010), Excellent Team of Scientific Research (201705), and the Foundation of A Hundred Youth Talents Training. We also express our thanks to the Instrument Analysis Center of LZJTU for the associated testing support.

REFERENCES

(1) Li, Y.; Zheng, N.; Yu, L.; Wen, S.; Gao, C.; Sun, M.; Yang, R. A Simple Phenyl Group Introduced at the Tail of Alkyl Side Chains of Small Molecular Acceptors: New Strategy to Balance the Crystallinity of Acceptors and Miscibility of Bulk Heterojunction Enabling Highly Efficient Organic Solar Cells. *Adv. Mater.* 2019, *31*, No. 1807832.

(2) Liu, T.; Luo, Z.; Fan, Q.; Zhang, G.; Zhang, L.; Gao, W.; Guo, X.; Ma, W.; Zhang, M.; Yang, C.; Li, Y.; Yan, H. Use of Two Structurally Similar Small Molecular Acceptors Enabling Ternary Organic Solar Cells with High Efficiencies and Fill Factors. *Energy Environ. Sci.* 2018, *11*, 3275−3282.

(3) Lv, J.; Feng, Y.; Fu, J.; Gao, J.; Singh, R.; Kumar, M.; Kim, M.; Tang, H.; Lu, S.; Zhang, W.; McCulloch, I.; Li, J.; Kan, Z. Energetic Disorder and Activation Energy in Efficient Ternary Organic Solar Cells with Nonfullerene Acceptor Eh-IDTBR as the Third Component. *Sol. RRL* 2019, No. 1900403.

(4) Liu, T.; Huo, L.; Chandrabose, S.; Chen, K.; Han, G.; Qi, F.; Meng, X.; Xie, D.; Ma, W.; Yi, Y.; Hodgkiss, J. M.; Liu, F.; Wang, J.; Yang, C.; Sun, Y. Optimized Fibril Network Morphology by Precise Side-Chain Engineering to Achieve High-Performance Bulk-Heterojunction Organic Solar Cells. *Adv. Mater.* 2018, *30*, No. 1707353.

(5) Chen, H.; Hu, D.; Yang, Q.; Gao, J.; Fu, J.; Yang, K.; He, H.; Chen, S.; Kan, Z.; Duan, T.; Yang, C.; Ouyang, J.; Xiao, Z.; Sun, K.; Lu, S. All-Small-Molecule Organic Solar Cells with an Ordered Liquid Crystalline Donor. *Joule* 2019, *3*, 3034−3047.

(6) Kang, Q.; Ye, L.; Xu, B.; An, C.; Stuard, S. J.; Zhang, S.; Yao, H.; Ade, H.; Hou, J. A Printable Organic Cathode Interlayer Enables over 13% Efficiency for 1-cm^2 Organic Solar Cells. *Joule* 2019, *3*, 227−239.

(7) Gao, K.; Miao, J.; Xiao, L.; Deng, W.; Kan, Y.; Liang, T.; Wang, C.; Huang, F.; Peng, J.; Cao, Y.; Liu, F.; Russell, T. P.; Wu, H.; Peng, X. Multi-Length-Scale Morphologies Driven by Mixed Additives in Porphyrin-Based Organic Photovoltaics. *Adv. Mater.* 2016, *28*, 4727−4733.

(8) Bao, X.; Zhang, Y.; Wang, J.; Zhu, D.; Yang, C.; Li, Y.; Yang, C.; Xu, J.; Yang, R. High Extinction Coefficient Thieno [3,4-b] thiophene-Based Copolymer for Efficient Fullerene-Free Solar Cells with Large Current Density. *Chem. Mater.* 2017, *29*, 6766−6771.

(9) Gao, K.; Li, L.; Lai, T.; Xiao, L.; Huang, Y.; Huang, F.; Peng, J.; Cao, Y.; Liu, F.; Russell, T. P.; Janssen, R. A. J.; Peng, X. Deep Absorbing Porphyrin Small Molecule for High-Performance Organic Solar Cells with Very Low Energy Losses. *J. Am. Chem. Soc.* 2015, *137*, 7282−7285.

(10) Kong, X.; Lin, H.; Du, X.; Li, L.; Li, X.; Chen, X.; Zheng, C.; Wang, D.; Tao, S. Hydrogen Bonds Induced High Performance Ternary Fullerene-Free Organic Solar Cells with Increased Current Density and Enhanced Stability. *J. Mater. Chem. C* 2018, *6*, 9691−9702.

(11) Du, Z.; Bao, X.; Li, Y.; Liu, D.; Wang, J.; Yang, C.; Wimmer, R.; Städ, L. W.; Yang, R.; Yu, D. Balancing High Open Circuit Voltage over 1.0 V and High Short Circuit Current in Benzodithiophene-Based Polymer Solar Cells with Low Energy Loss: A Synergistic Effect of Fluorination and Alkylthiolation. *Adv. Energy Mater.* 2018, *8*, No. 1701471.

(12) Duan, T.; Tang, H.; Liang, R.; Lv, J.; Kan, Z.; Singh, R.; Kumar, M.; Xiao, Z.; Lu, S.; Laquai, F. Terminal Group Engineering for Small-Molecule Donors Boosts the Performance of Nonfullerene Organic Solar Cells. *J. Mater. Chem. A* 2019, *7*, 2541−2546.

(13) Gao, K.; Jo, S. B.; Shi, X.; Nian, L.; Zhang, M.; Kan, Y.; Lin, F.; Kan, B.; Xu, B.; Rong, Q.; Shui, L.; Liu, F.; Peng, X.; Zhou, G.; Cao, Y.; Jen, A. K.-Y. Over 12% Efficiency Nonfullerene All-Small-Molecule Organic Solar Cells with Sequentially Evolved Multilength Scale Morphologies. *Adv. Mater.* 2019, *31*, No. 1807842.

(14) Tong, J.; An, L.; Lv, J.; Guo, P.; Wang, X.; Yang, C.; Xia, Y. Enhanced Photovoltaic Performance in D-π-ACopolymers Containing Triisopropylsilylethynyl-Substituted Dithienobenzodithiophene by Modulating the Electron-Deficient Units. *Polymers* 2019, *11*, No. 12.

(15) Yu, L.; Li, Y.; Wang, Y.; Wang, X.; Cui, W.; Wen, S.; Zheng, N.; Sun, M.; Yang, R. Fuse the π-Bridge to Acceptor Moiety of Donor-π-Acceptor Conjugated Polymer: Enabling an All-Round Enhancement in Photovoltaic Parameters of Nonfullerene Organic Solar Cells. *ACS Appl. Mater. Interfaces* 2019, *11*, 31087−31095.

(16) Dou, K.; Wang, X.; Du, Z.; Jiang, H.; Li, F.; Sun, M.; Yang, R. Synergistic Effect of Side-Chain and Backbone Engineering in Thieno[2,3-f]benzofuran-Based Conjugated Polymers for High Performance Non-Fullerene Organic Solar Cells. *J. Mater. Chem. A* 2019, *7*, 958−964.

(17) Wang, X.; Yao, Y.; Jing, X.; Li, F.; Yu, L.; Hao, Y.; Sun, M. Thiophene Copolymer for 1 V High Open-Circuit Voltage Semi-transparent Photovoltaic Devices. *J. Mater. Chem. C* 2019, *7*, 10868−10875.

(18) Tan, H.; Zheng, X.; Zhu, J.; Yu, J.; Zhu, W. An A−D−D−A-type Non-fullerene Small-Molecule Acceptor with Strong Near-infrared Absorption for High Performance Polymer Solar Cells. *J. Mater. Chem. C* 2019, *7*, 13301−13306.

(19) Peng, W.; Zhang, G.; Shao, L.; Ma, C.; Zhang, B.; Chi, W.; Peng, Q.; Zhu, W. Simple-Structured Small Molecule Acceptors Constructed by a Weakly Electron-Deficient Thiazolothiazole Core for High-Efficiency Non-Fullerene Organic Solar Cells. *J. Mater. Chem. A* 2018, *6*, 24267−24276.

(20) An, L.; Tong, J.; Yang, C.; Zhao, X.; Wang, X.; Xia, Y. Impact of Alkyl Side Chain on the Photostability and Optoelectronic Properties of Indacenodithieno[3,2-*b*]thiophene-*alt*-naphtho[1,2-*c*:5,6-*c*′]bis-[1,2,5]thiadiazole Medium Bandgap Copolymers. *Polym. Int.* 2020, *69*, 192−205.

(21) Tan, H.; Long, Y.; Zhang, J.; Zhu, J.; Yang, J.; Yu, J.; Zhu, W. Spirobifluorene-Cored Wide Bandgap Non-Fullerene Small Molecular Acceptor with 3D Structure for Organic Solar Cells. *Dyes Pigm.* 2019, *162*, 797−801.

(22) Chen, W.; Shen, W.; Wang, H.; Liu, F.; Duan, L.; Xu, X.; Zhu, D.; Qiu, M.; Wang, E.; Yang, R. Enhanced Efficiency of Polymer Solar Cells by Improving Molecular Aggregation and Broadening the Absorption Spectra. *Dyes Pigm.* 2019, *166*, 42−48.

(23) Liu, T.; Gao, W.; Wang, Y.; Yang, T.; Ma, R.; Zhang, G.; Zhong, C.; Ma, W.; Yan, H.; Yang, C. Unconjugated Side-Chain Engineering Enables Small Molecular Acceptors for Highly Efficient Non-Fullerene Organic Solar Cells: Insights into the Fine-Tuning of Acceptor Properties and Micromorphology. *Adv. Funct. Mater.* 2019, *29*, No. 1902155.

(24) Luo, Z.; Liu, T.; Wang, Y.; Zhang, G.; Sun, R.; Chen, Z.; Zhong, C.; Wu, J.; Chen, Y.; Zhang, M.; Zou, Y.; Ma, W.; Yan, H.; Min, J.; Li, Y.; Yang, C. Reduced Energy Loss Enabled by a Chlorinated Thiophene-Fused Ending-Group Small Molecular Acceptor for Efficient Non-fullerene Organic Solar Cells with 13.6% Efficiency. *Adv. Energy Mater.* 2019, *9*, No. 1900041.

(25) Jo, J. W.; Jung, J. W.; Ahn, H.; Ko, M. J.; Jen, A. K.-Y.; Son, H. J. Effect of Molecular Orientation of Donor Polymers on Charge Generation and Photovoltaic Properties in Bulk Heterojunction All-Polymer Solar Cells. *Adv. Energy Mater.* 2017, *7*, No. 1601365.

(26) Shin, I.; Ahn, Hj.; Yun, J. H.; Jo, J. W.; Park, S.; Joe, S.-y.; Bang, J.; Son, H. J. High-Performance and Uniform 1 cm^2 Polymer Solar Cells with D1-A-D2-A-Type Random Terpolymers. *Adv. Energy Mater.* 2018, *8*, No. 1701405.

(27) Yao, H.; Li, Y.; Hu, H.; Chow, P. C. Y.; Chen, S.; Zhao, J.; Li, Z.; Carpenter, J. H.; Lai, J. Y. L.; Yang, G.; Liu, Y.; Lin, H.; Ade, H.; Yan, H. A Facile Method to Fine-Tune Polymer Aggregation Properties and Blend Morphology of Polymer Solar Cells Using Donor Polymers with Randomly Distributed Alkyl Chains. *Adv. Energy Mater.* 2018, *8*, No. 1701895.

(28) Wang, X.; Du, Z.; Dou, K.; Jiang, H.; Gao, C.; Han, L.; Yang, R. A Maverick Asymmetrical Backbone with Distinct Flanked Twist Angles Modulating the Molecular Aggregation and Crystallinity for High Performance Nonfullerene Solar Cells. *Adv. Energy Mater.* 2019, *9*, No. 1802530.

(29) Wang, X.; Dou, K.; Shahid, B.; Liu, Z.; Li, Y.; Sun, M.; Zheng, N.; Bao, X.; Yang, R. Terpolymer Strategy toward High-Efficiency Polymer Solar Cells: Integrating Symmetric Benzodithiophene and Asymmetrical Thieno[2,3-f] benzofuran Segments. *Chem. Mater.* 2019, *31*, 6163−6173.

https://dx.doi.org/10.1021/acsami.9b20364
ACS Appl. Mater. Interfaces 2020, 12, 8475−8484

(30) Kang, T. E.; Kim, K.-H.; Kim, B. J. Design of Terpolymers as Electron Donors for Highly Efficient Polymer Solar Cells. *J. Mater. Chem. A* 2014, *2*, 15252−15267.
(31) Xu, X.; Bi, Z.; Ma, W.; Zhang, G.; Yan, H.; Li, Y.; Peng, Q. Stable Large Area Organic Solar Cells Realized by using Random Terpolymers Donors Combined with a Ternary Blend. *J. Mater. Chem. A* 2019, *7*, 14199−14208.
(32) Kim, D. H.; Trang Bui, T. T.; Rasool, S.; Song, C. E.; Lee, H. K.; Lee, S. K.; Lee, J.-C.; So, W.-W.; Shin, W. S. High-Efficiency Nonfullerene Polymer Solar Cells with Band gap and Absorption Tunable Donor/Acceptor Random Copolymers. *ACS Appl. Mater. Interfaces* 2019, *11*, 2189−2196.
(33) Lee, Y.; Aplan, M. P.; Seibers, Z. D.; Xie, R.; Culp, T. E.; Wang, C.; Hexemer, A.; Kilbey, S. M.; Wang, Q.; Gomez, E. D. Random Copolymers Allow Control of Crystallization and Microphase Separation in Fully Conjugated Block Copolymers. *Macromolecules* 2018, *51*, 8844−8852.
(34) Wang, X.; Deng, W.; Chen, Y.; Wang, X.; Ye, P.; Wu, X.; Yan, C.; Zhan, X.; Liu, F.; Huang, H. Fine-Tuning Solid State Packing and Significantly Improving Photovoltaic Performance of Conjugated Polymers Through Side Chain Engineering via Random Polymerization. *J. Mater. Chem. A* 2017, *5*, 5585−5593.
(35) Huang, G.; Zhang, J.; Uranbileg, N.; Chen, W.; Jiang, H.; Tan, H.; Zhu, W.; Yang, R. Significantly Enhancing the Efficiency of a New Light-Harvesting Polymer with Alkylthio naphthyl Substituents Compared to Their Alkoxyl Analogs. *Adv. Energy Mater.* 2018, *8*, No. 1702489.
(36) Li, J.; Wang, Y.; Liang, Z.; Wang, N.; Tong, J.; Yang, C.; Bao, X.; Xia, Y. Enhanced Organic Photovoltaic Performance through Modulating Vertical Composition Distribution and Promoting Crystallinity of the Photoactive Layer by Diphenyl Sulfide Additives. *ACS Appl. Mater. Interfaces* 2019, *11*, 7022−7029.
(37) Wang, Y.; Liang, Z.; Qin, J.; Tong, J.; Guo, P.; Cao, X.; Li, J.; Xia, Y. An Alcohol-soluble Polymer Electron Transport Layer Based on Perylene Diimide Derivatives for Polymer Solar Cells. *IEEE J. Photovoltaics* 2019, *9*, 1678−1685.
(38) Li, J.; Wang, Y.; Liang, Z.; Qin, J.; Ren, M.; Tong, J.; Yang, C.; Yang, C.; Bao, X.; Xia, Y. Non-Toxic Green Food Additive Enables Efficient Polymer Solar Cells Through Adjusting Phase Composition Distribution and Boosting Charge Transport. *J. Mater. Chem. C* 2020, DOI: 10.1039/C9TC06571G.
(39) Wang, Y.; Liang, Z.; Li, X.; Qin, J.; Ren, M.; Yang, C.; Bao, X.; Xia, Y.; Li, J. Self-Doping n-Type Polymer as a Cathode Interface Layer Enables Efficient Organic Solar Cells by Increasing Built-in Electric Field and Boosting Interface Contact. *J. Mater. Chem. C* 2019, *7*, 11152−11159.
(40) Li, X.; Liang, Z.; Wang, H.; Qiao, S.; Liu, Z.; Jiang, H.; Chen, W.; Yang, R. Fluorinated D1(0.5)−A−D2(0.5)−A Model Terpolymer: Ultrafast Charge Separation Kinetics and Electron Transfer at Fluorinated D/A Interface for Power Conversion. *J. Mater. Chem. A* 2020, *8*, 1360−1367.
(41) Li, J.; Wang, N.; Wang, Y.; Liang, Z.; Peng, Y.; Yang, C.; Bao, X.; Xia, Y. Efficient Inverted Organic Solar Cells with a Thin Natural Biomaterial L-Arginine as Electron Transport Layer. *Sol. Energy* 2020, *196*, 168−176.
(42) Tang, H.; Xu, T.; Yan, C.; Gao, J.; Yin, H.; Lv, J.; Singh, R.; Kumar, M.; Duan, T.; Kan, Z.; Lu, S.; Li, G. Donor Derivative Incorporation: An Effective Strategy toward High Performance All-Small-Molecule Ternary Organic Solar Cells. *Adv. Sci.* 2019, *6*, No. 1901613.
(43) Li, J.; Liang, Z.; Wang, Y.; Li, H.; Tong, J.; Bao, X.; Xia, Y. Enhanced Efficiency of Polymer Solar Cells Through Synergistic Optimization of Mobility and Tuning Donor Alloys by Adding High-Mobility Conjugated Polymers. *J. Mater. Chem. C* 2018, *6*, 11015−11022.
(44) Du, X.; Lu, X.; Zhao, J.; Zhang, Y.; Li, X.; Lin, H.; Zheng, C.; Tao, S. Hydrogen Bond Induced Green Solvent Processed High Performance Ternary Organic Solar Cells with Good Tolerance on Film Thickness and Blend Ratios. *Adv. Funct. Mater.* 2019, *29*, No. 1902078.
(45) Liang, Z.; Tong, J.; Li, H.; Wang, Y.; Wang, N.; Li, J.; Yang, C.; Xia, Y. The Comprehensive Utilization of the Synergistic Effect of Fullerene and Non-Fullerene Acceptors to Achieve Highly Efficient Polymer Solar Cells. *J. Mater. Chem. A* 2019, *7*, 15841−15850.
(46) Zhang, X.; Zhang, D.; Zhou, Q.; Wang, R.; Zhou, J.; Wang, J.; Zhou, H.; Zhang, Y. Fluorination with an Enlarged Dielectric Constant Prompts Charge Separation and Reduces Bimolecular Recombination in Non-Fullerene Organic Solar Cells with a High Fill Factor and Efficiency > 13%. *Nano Energy* 2019, *56*, 494−501.
(47) Zalar, P.; Kuik, M.; Ran, N. A.; Love, J. A.; Nguyen, T.-Q. Effects of Processing Conditions on the Recombination Reduction in Small Molecule Bulk Heterojunction Solar Cells. *Adv. Energy Mater.* 2014, *4*, No. 1400438.
(48) Zhang, X.; Zuo, X.; Xie, S.; Yuan, J.; Zhou, H.; Zhang, Y. Understanding Charge Transport and Recombination Losses in High Performance Polymer Solar Cells with Non-Fullerene Acceptors. *J. Mater. Chem. A* 2017, *5*, 17230−17239.
(49) Wetzelaer, G.-J. A. H.; Van der Kaap, N. J.; Koster, L. J. A.; Blom, P. W. M. Quantifying Bimolecular Recombination in Organic Solar Cells in Steady State. *Adv. Energy Mater.* 2013, *3*, 1130−1134.
(50) Barone, V.; Cossi, M. Quantum Calculation of Molecular Energies and Energy Gradients in Solution by a Conductor Solvent Model. *J. Phys. Chem. A* 1998, *102*, 1995−2001.
(51) Moellmann, J.; Grimme, S. DFT-D3 Study of Some Molecular Crystals. *J. Phys. Chem. C* 2014, *118*, 7615−7621.
(52) Smith, D. G. A.; Burns, L. A.; Patkowski, K.; Sherrill, C. D. Revised Damping Parameters mfor the D3 Dispersion Correction to Density Functional Theory. *J. Phys. Chem. Lett.* 2016, *7*, 2197−2203.
(53) Franceschetti, A.; Zunger, A. Direct Pseudopotential Calculation of Exciton Coulomb and Exchange Energies in Semiconductor Quantum Dots. *Phys. Rev. Lett.* 1997, *78*, No. 915.
(54) Zhang, Y.; Basu, K.; Canary, J. W.; Jerschow, A. Singlet Lifetime Measurements in an All-Proton Chemically Equivalent Spin System by Hyperpolarization and Weak Spin Lock Transfers. *Phys. Chem. Chem. Phys.* 2015, *17*, 24370−24375.
(55) Köse, M. E. Evaluation of Acceptor Strength in Thiophene Coupled Donor−Acceptor Chromophores for Optimal Design of Organic Photovoltaic Materials. *J. Phys. Chem. A* 2012, *116*, 12503−12509.
(56) Heremans, P.; Cheyns, D.; Rand, B. P. Strategies for Increasing the Efficiency of Heterojunction Organic Solar Cells: Material Selection and Device Architecture. *Acc. Chem. Res.* 2009, *42*, 1740−1747.
(57) Wang, D.; Ding, W.; Geng, Z.; Wang, L.; Geng, Y.; Su, Z.; Yu, H. Rational Design and Characterization of High-Efficiency Planar A−π−D−π−A Type Electron Donors in Small Molecule Organic Solar Cells: A Quantum Chemical Approach. *Mater. Chem. Phys.* 2014, *145*, 387−396.
(58) Ding, W.-L.; Wang, D.-M.; Geng, Z.-Y.; Zhao, X.-L.; Yan, Y.-F. Molecular Engineering of Indoline-Based D−A−π−A Organic Sensitizers toward High Efficiency Performance from First-Principles Calculations. *J. Phys. Chem. C* 2013, *117*, 17382−17398.
(59) Jamieson, F. C.; Domingo, E. B.; McCarthy-Ward, T.; Heeney, M.; Stingelin, N.; Durrant, J. R. Fullerene Crystallisation as a Key Driver of Charge Separation in Polymer/Fullerene Bulk Heterojunction Solar Cells. *Chem. Sci.* 2012, *3*, 485−492.
(60) Collado-Fregoso, E.; Boufflet, P.; Fei, Z.; Gann, E.; Ashraf, S.; Li, Z.; McNeill, C. R.; Durrant, J. R.; Heeney, M. Increased Exciton Dipole Moment Translates into Charge-Transfer Excitons in Thiophene-Fluorinated Low-Bandgap Polymers for Organic Photovoltaic Applications. *Chem. Mater.* 2015, *27*, 7934−7944.
(61) Mikhnenko, O. V.; Azimi, H.; Scharber, M.; Morana, M.; Blom, P. W. M.; Loi, M. A. Exciton Diffusion Length in Narrow Bandgap Polymers. *Energy Environ. Sci.* 2012, *5*, 6960−6965.
(62) Kang, T. E.; Kim, K. H.; Kim, B. J. Design of Terpolymers as Electron Donors for Highly Efficient Polymer Solar Cells. *J. Mater. Chem. A* 2014, *2*, 15252−15267.
(63) Feng, H.; Qiu, N.; Wang, X.; Wang, Y.; Kan, B.; Wan, X.; Zhang, M.; Xia, A.; Li, C.; Liu, F.; Zhang, H.; Chen, Y. An A-D-A Type Small-

Molecule Electron Acceptor with End-Extended Conjugation for High Performance Organic Solar Cells. *Chem. Mater.* 2017, *29*, 7908−7917.
(64) Liu, X.; Yan, Y.; Honarfar, A.; Yao, Y.; Zheng, K.; Liang, Z. Unveiling Excitonic Dynamics in High-Efficiency Nonfullerene Organic Solar Cells to Direct Morphological Optimization for Suppressing Charge Recombination. *Adv. Sci.* 2019, *6*, No. 1802103.
(65) Zídek, K.; Zheng, K.; Ponseca, C. S.; Messing, M. E.; Wallenberg, L. R.; Chábra, P.; Abdellah, M.; Sundström, V.; Pullerits, T. Electron Transfer in Quantum-Dot-Sensitized ZnO Nanowires: Ultrafast Time-Resolved Absorption and Terahertz Study. *J. Am. Chem. Soc.* 2012, *134*, 12110−12117.

https://dx.doi.org/10.1021/acsami.9b20364
ACS Appl. Mater. Interfaces 2020, 12, 8475−8484